11-1-2020

A novel STING1 variant causes a recessive form of STING-associated vasculopathy with onset in infancy (SAVI).

Bin Lin

Roberta Berard
Department of Pediatrics, Western University, London, Ontario,Canada, rberard2@uwo.ca

Abdulrahman Al Rasheed

Buthaina Aladba

Philip J Kranzusch

See next page for additional authors

Cdc42.[4,5] In our study, the doubly lipidated R186C Cdc42 mutant was retained in the Golgi (see Fig E4, *B*). This impaired its plasma membrane anchoring and resulted in actin polymerization defects and hyperactivation of NF-κB signaling.

In conclusion, our study identifies a strong link between impaired cytosol/membrane cycling of Cdc42 resulting from abnormal double lipidation, partial defects in actin polymerization, and hyperactivation of NF-κB signaling, which can explain the pathophysiology of the disease. More broadly, our findings are consistent with reports in the literature that link inflammation with actin turnover[6] and membrane targeting of Rho GTPases.[7-9] Thus, further investigation of the various consequences of *CDC42* mutations are required because these mutations arise in a broad spectrum of clinical phenotypes. Ultimately, it offers the possibility of designing specific therapeutic targeting of this pathway that is newly involved in autoinflammatory diseases.

We thank patient A.S. and his family for participating in this research.

Bahia Bekhouche, MSc[a]*
Aurore Tourville, MSc[b]*
Yamini Ravichandran, MTech[c,d]
Rachida Tacine, BSc[b]
Laurence Abrami, PhD[e]
Michael Dussiot, MSc[a]
Andrea Khau-Dancasius, MD[a]
Olivia Boccara, MD[f]
Meriem Khirat, MD[b]
Marianne Mangeney, PhD[b]
Florent Dingli, MSc[g]
Damarys Loew, PhD[g]
Batiste Boëda, PhD[c]
Pénélope Jordan, MD[h]
Thierry Jo Molina, MD, PhD[a,i]
Nathalia Bellon, MD[f]
Sylvie Fraitag, MD[j]
Smail Hadj-Rabia, MD, PhD[f]
Stéphane Blanche, MD, PhD[k]
Anne Puel, PhD[l]
Sandrine Etienne-Manneville, PhD[c]
F. Gisou van der Goot, PhD[e]
Jacqueline Cherfils, PhD[m]
Olivier Hermine, MD, PhD[a,n]
Jean-Laurent Casanova, MD, PhD[l,o,p]
Christine Bodemer, MD, PhD[f]‡
Asma Smahi, PhD[a]‡
Jérôme Delon, PhD[b]‡

From [a]the Institut Imagine, INSERM U1163, CNRS ERL 8254, Université Paris Descartes, Sorbonne Paris-Cité, Laboratoire d'Excellence GR-Ex, Paris, France; [b]the Université de Paris, Institut Cochin, INSERM, U1016, CNRS, UMR8104, Paris, France; [c]the Cell Polarity, Migration and Cancer Unit, Institut Pasteur, UMR3691 CNRS, Equipe Labellisée Ligue Contre le Cancer, Paris, France; [d]Sorbonne Université, Collège doctoral, F-75005 Paris, France; [e]the Global Health Institute, School of Life Sciences, EPFL, Lausanne, Switzerland; [f]the Department of Dermatology, Reference Center for Genodermatoses (MAGEC), Necker- Enfants Malades Hospital (AP-HP), Paris Descartes-Sorbonne Paris Cité University, Imagine Institute, Paris, France; [g]the Institut Curie, PSL Research University, Centre de Recherche, Laboratoire de Spectrométrie de Masse Protéomique, Paris, France; [h]the Fédération de Génétique, Service de Génétique Moléculaire, Hôpital Necker-Enfants Malades, Paris, France; [i]the Department of Pathology, Necker Enfants Malades, Université de Paris, France; [j]the Department of Pathology, reference centre MAGEC, Necker-Enfants Malades Hospital, APHP; [k]Unité d'Immunologie Hématologie Rhumatologie Pédiatrique, Necker-Enfants Malades Hospital (AP-HP5), Paris Descartes-Sorbonne Paris Cité University, France; [l]the Laboratory of Human Genetics of Infectious Diseases, Necker Branch, INSERM U1163, Descartes University, Imagine Institute, Paris, France; [m]the Laboratoire de Biologie et Pharmacologie Appliquée, CNRS and Ecole Normale Supérieure Paris-Saclay, Cachan, France; [n]the Department of Hematology, Hôpital Necker AP-HP, Paris, France; [o]the St. Giles Laboratory of Human Genetics of Infectious Diseases, Rockefeller Branch, Rockefeller University, New York, NY, Howard Hughes Medical Institute, New York, NY; and [p]the Department of Pediatric Immunology and Hematology, Necker-Enfants Malades Hospital (AP-HP), Paris Descartes-Sorbonne Paris Cité University, Paris, France. E-mail: christine.bodemer@aphp.fr. Or: asma.smahi@inserm.fr. Or: jerome.delon@inserm.fr.

*These authors contributed equally to this work as first authors.

‡These authors contributed equally to this work.

Supported by INSERM, CNRS, Université de Paris, Association pour la Recherche contre le Cancer (to J.D.), Ligue Contre le Cancer (to S.E.M.), Société Française de Dermatologie (to A.S., C.B., and J.D.), Agence Nationale de la Recherche (RIDES to A.S., J.D., and J.C.), the European Union Horizon 2020 Marie Skłodowska-Curie research and innovation program (MSCA-ITN-2015-675407 to S.E.M.), Institut Pasteur, the Région Ile de France and the Fondation pour la Recherche Médicale (J.C. and D.L.).

Disclosure of potential conflict of interest: The authors declare that they have no relevant conflicts of interest.

REFERENCES

1. Rougerie P, Delon J. Rho GTPases: masters of T lymphocyte migration and activation. Immunol Lett 2012;142:1-13.
2. Cherfils J, Zeghouf M. Regulation of small GTPases by GEFs, GAPs, and GDIs. Physiol Rev 2013;93:269-309.
3. Hoffman GR, Nassar N, Cerione RA. Structure of the Rho family GTP-binding protein Cdc42 in complex with the multifunctional regulator RhoGDI. Cell 2000;100:345-56.
4. Gernez Y, de Jesus AA, Alsaleem H, Macaubas C, Roy A, Lovell D, et al. Severe autoinflammation in 4 patients with C-terminal variants in cell division control protein 42 homolog (CDC42) successfully treated with IL-1β inhibition. J Allergy Clin Immunol 2019;144:1122-5.
5. Lam MT, Coppola S, Krumbach OHF, Prencipe G, Insalaco A, Cifaldi C, et al. A novel disorder involving dyshematopoiesis, inflammation, and HLH due to aberrant CDC42 function. J Exp Med 2019;216:2778-99.
6. Pfajfer L, Mair NK, Jimenez-Heredia R, Genel F, Gulez N, Ardeniz O, et al. Mutations affecting the actin regulator WD repeat-containing protein 1 lead to aberrant lymphoid immunity. J Allergy Clin Immunol 2018;142:1589-604.e11.
7. Akula MK, Shi M, Jiang Z, Foster CE, Miao D, Li AS, et al. Control of the innate immune response by the mevalonate pathway. Nat Immunol 2016;17:922-9.
8. Park YH, Wood G, Kastner DL, Chae JJ. Pyrin inflammasome activation and RhoA signaling in the autoinflammatory diseases FMF and HIDS. Nat Immunol 2016;17:914-21.
9. Akula MK, Ibrahim MX, Ivarsson EG, Khan OM, Kumar IT, Erlandsson M, et al. Protein prenylation restrains innate immunity by inhibiting Rac1 effector interactions. Nat Commun 2019;3975.

Available online April 10, 2020.
https://doi.org/10.1016/j.jaci.2020.03.020

A novel *STING1* variant causes a recessive form of STING-associated vasculopathy with onset in infancy (SAVI)

To the Editor:

Stimulator of interferon response genes (STING) encoded by stimulator of interferon response cGAMP interactor 1 (*STING1*), previously known as transmembrane protein 173 (*TMEM173*) is an important pattern recognition receptor that detects microbial dinucleotides and functions as an adaptor molecule in the cytosolic DNA sensing pathway that binds 2'3'-cyclic GMP-AMP (cGAMP), which is generated when cytosolic DNA activates

cyclic GMP-AMP synthase (cGAS).[1,2] STING activation stimulates the induction of type I interferons, which activate interferon responses. Gain-of-function (GOF) variants in *STING1* lead to autoactivation without ligand binding and cause a rare autoinflammatory disease named STING-associated vasculopathy with onset in infancy (SAVI) (Online Mendelian Inheritance in Man catalog no. 615934).[3,4] Patients with SAVI present in infancy with the following symptoms: recurrent fevers; cold-induced skin vasculitis that can progress to tissue loss and amputation of fingers and toes; and/or interstitial lung disease, which is the main cause of the mortality that often occurs before patients reach adulthood. So far, all reported cases of SAVI have been caused by autosomal dominant variants, with most of them occurring *de novo*.

We have identified 6 patients from 4 unrelated families, all of whom are of Arabic ethnicity and harbor pathogenic *STING1* variants that are disease causing only in homozygosity. The patients had clinical disease suggestive of SAVI and were enrolled into institutional review board–approved protocols, including the National Institutes of Health natural history protocol (NCT02974595).

Patient 1, the index patient, presented at 4 weeks of age with a cough and failure to thrive, as well as with a maculopapular violaceous rash with a livedoid appearance (Fig 1, *A* and *B*). A chest computed tomography scan showed diffuse bilateral parenchymal opacities. His lung disease progressed despite steroid therapy and short-term treatment with the JAK inhibitor tofacitinib, and he died of respiratory failure at 5 months of age. His older brother (patient 2) died at 18 months of age with chronic cough and failure to thrive. Although genetic testing was not performed, the clinical manifestations and similarities of patient 2 to those of his younger brother strongly suggest that he had SAVI. Patient 3 presented at 3 months of age with recurrent fever, erythematous rash, cough, and dyspnea, ultimately progressing to oxygen dependence. He had a chest computed tomography scan with results consistent with interstitial lung disease and a lung biopsy specimen that showed chronic interstitial pneumonitis with intraalveolar hemorrhage. He is currently taking the JAK inhibitor ruxolitinib. His brother, patient 4, had respiratory symptoms starting at the age of 6 months; he was diagnosed with SAVI at the age of 15 months and was initially treated with steroids, after which baricitinib (a selective JAK1/2 inhibitor) was added to his treatment regimen. Patient 5 presented at the age of 2 months with cough, tachypnea, and recurrent lung infections; she was diagnosed with chronic aspiration pneumonia and had a laryngeal cleft that was repaired at the age of 4.5 years. Because of her lung disease (Fig 1, *E*), she has required supplemental oxygen since the age of 7 months and bilevel positive airway pressure support while sleeping since the second year of life, when digital clubbing was noticed. She developed pulmonary hypertension by the age of 4 years. At the age of 5 she developed polyarthritis, an erythematous rash over the soles of her feet and clubbing. She began taking baricitinib at the age of 7 years; there was clinical improvement, but her oxygen dependence continued. Patient 6 presented at the age of 8 months with a history of persistent tachypnea and failure to thrive, polyarthritis, intermittent vasculitic rashes, and clubbing (Fig 1, *C* and *D*). All of the parents and siblings were asymptomatic with normal inflammatory markers. Additional clinical and laboratory information is available in Table E1 (in this article's Online Repository at www.jacionline.org).

Patients 1, 3, and 4 underwent targeted sequencing of *STING1*, whereas whole exome sequencing was performed on families 3 and 4. Sequencing of all patients revealed a homozygous *STING1* (NM_198282) variant c.841C>T, p.Arg281Trp, p.R281W (Fig 1, F). This variant was present in heterozygosity in only 2 of 282,822 alleles reported in gnomAD (gnomad.broadinstitute.org) and is predicted to be damaging by PolyPhen-2 and deleterious by the scale-invariant feature transform algorithm (SIFT), and it has a Combined Annotation-Dependent Depletion (CADD)-PHRED-scaled score of 26.4. This variant has not been reported previously in patients with SAVI (https://infevers.umai-montpellier.fr). All of the parents, as well as several of the unaffected siblings, were heterozygous carriers of this variant (Fig 1, *F*). A variant affecting the same amino acid residue but mutated to a glutamine (c.842G>A, p.Arg281Gln, p.R281Q) has previously been described to cause an autosomal dominant form of SAVI[5] (Fig 1, *G*).

A strikingly high interferon response gene signature and systemic inflammation in patients with SAVI has led to their designation as having an autoinflammatory interferonopathy.[6] A standardized interferon response gene score was elevated only in patients who were homozygous for the p.R281W variant and who had clinical disease, and not in the siblings and parents who were heterozygous carriers of the variant or in healthy controls (Fig 1, *H*).

Transfection of HEK293T cells with the *STING1* construct containing the R281W mutation led to activation of *IFNB1* luciferase reporter without ligand binding (see Fig E1 in this article's Online Repository at www.jacionline.org), indicating that p.R281W is a pathogenic GOF variant. The mutant remained responsive to cGAMP (see Fig E1), suggesting no effect on ligand binding.

Disease-causing SAVI variants[3] cluster in 2 areas. The cryoelectron microscopy structure model of STING[7] has mapped the class 1 variants, p.N154S, p.V155M, and p.V147L to the connector helix loop (Fig 1, *G*) which controls a cGAMP ligand–induced 180° rotation of the ligand-binding area of the STING dimer that induces polymerization and activation. The class 3 variants, including p.R281Q, p.R284G[5] and p.R284S,[8] are located at the polymerization interface[7] (Fig 1, *G*) and have been postulated to bind a C-terminal tail that might prevent polymerization and autoactivation.[9]

Concordant with previous reports, we hypothesized that the p.R281W variant confers a GOF that is weaker than the heterozygous SAVI variants. To test this possibility, we transfected HEK293T cells with either wild-type or mutant STING constructs including R281W at increasing concentrations and assessed *IFNB1* reporter activity (Fig 2, *A*). At equal transfection efficiency, consistent with the homozygosity requirement at this location, R281W mutant constructs exhibited lower autoactivation than R281Q constructs did but were similar to mutant constructs with the pathogenic V155M variant. This suggests differential autoactivation thresholds for disease-causing class 1 variants at the connector helix loop (ie, V155M) versus class 3 variants at the polymer interface (ie, R281 and R284). In line with this hypothesis, pathogenic variants at the class 3 residues that cause disease in heterozygosity, including R281Q, R284S, and R284G, are all more autoactivating than V155M in the transfection model (Fig 2, *A* and *B*), with R284S, R284G, and G158A constituting the top 3 autoactivating SAVI variants (Fig 2, *B*).

Although class 1 disease-causing SAVI variants are GOF variants, mutating these residues into charged amino acids

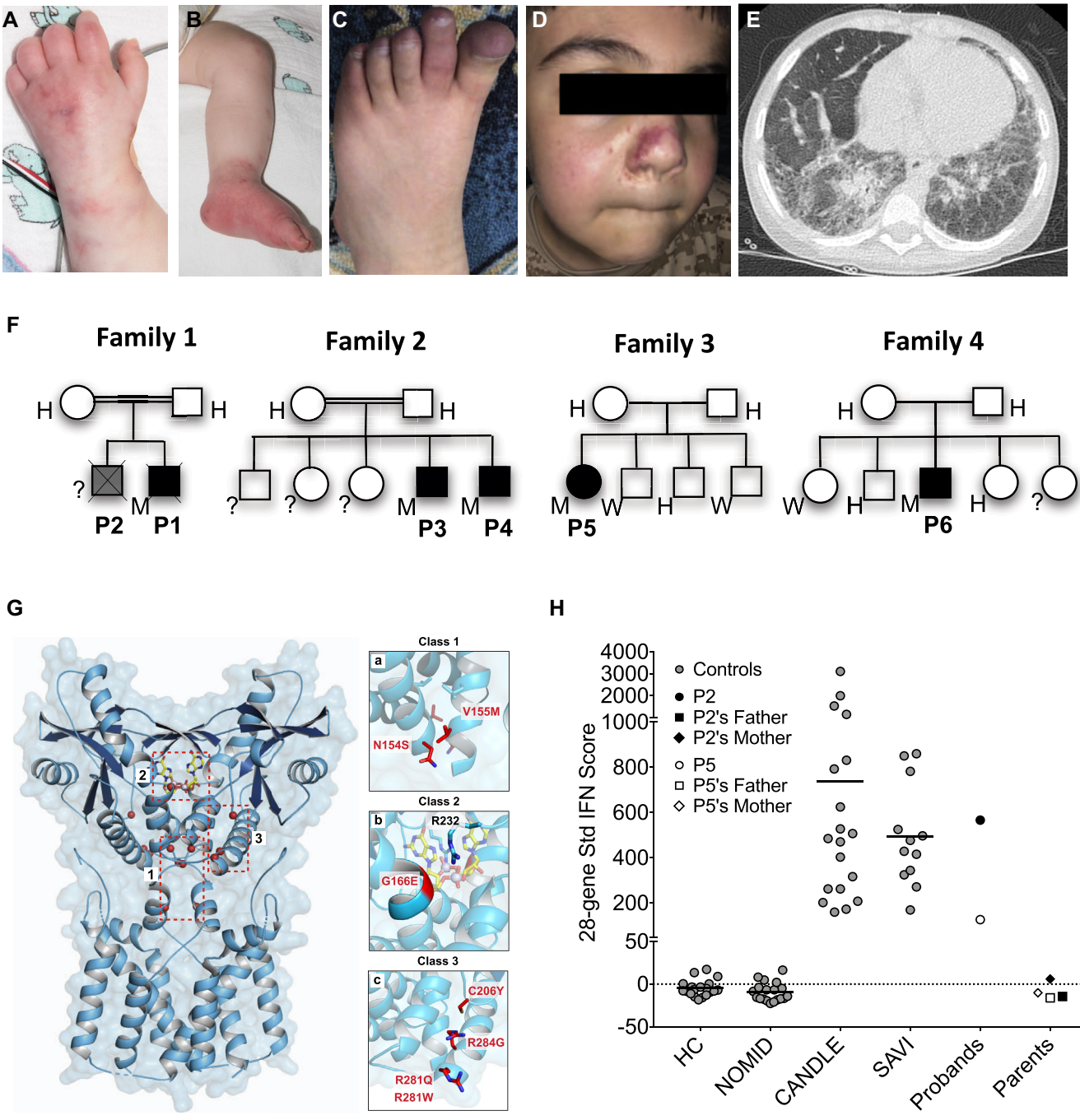

FIG 1. Homozygous *STING1* variant p.R281W causes SAVI. **A-E**, Clinical images showing typical cutaneous features of vasculopathy for patient 1 (P1) (*A* and *B*) and P6 (*C* and *D*), as well as a chest computed tomography scan (**E**) demonstrating reticulonodular densities throughout (P5). **F,** Family trees. **G,** Location of p.R281W and other disease-causing SAVI mutations in the cryoelectron microscopy structure model of STING. Highlighted are previously reported class 1 mutations in the connector helix loop, class 2 mutation in the cGAMP binding pocket, and class 3 mutations on a surface-exposed region of STING dimer. **H,** Interferon (IFN) scores of p.R281W homozygous patients and their parents compared with those of healthy controls (HCs) or patients with neonatal-onset multisystem inflammatory disease (NOMID), chronic atypical neutrophilic dermatosis with lipodystrophy and elevated temperature (CANDLE), or SAVI with heterozygous GOF *STING1* mutations. *H,* Heterozygous; *M,* homozygous; *Std,* standard; *W,* wild type.

(eg, V155R[3] and G158E[8]) leads to loss of function, likely through destabilizing the STING dimer structure. In contrast, none of the 6 different amino acid mutations at position R281 caused loss of function (Fig 2, *B* [*green labels*]). In fact, all of the mutations except for R281A, which is similar to the wild type, led to autoactivation. Maintenance of a positive charge at residue R281 (by mutating into lysine [K] or histidine [H]) was insufficient to keep STING inactive at the basal state. Moreover,

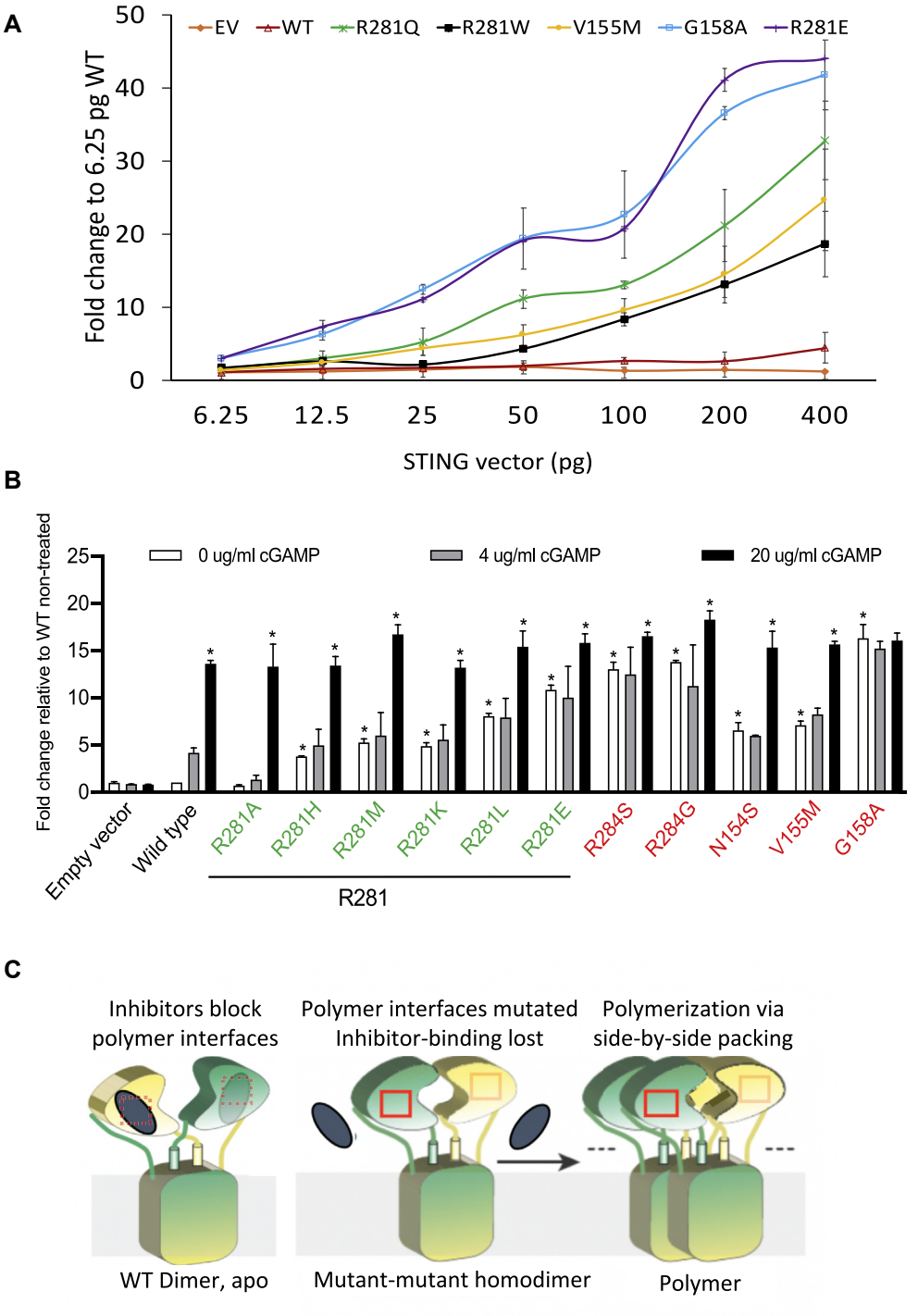

FIG 2. Multiple random *STING1* mutations at p.R281 lead to strong autoactivation. **A,** *IFNB1* reporter activation by R281W and other STING constructs transfected into HEK293T cells at increasing concentrations. **B,** R281 mutations led to strong STING autoactivation, as measured by *IFNB1* reporter activation in HEK293T cells. In particular, R281E was superactivating, comparable to the most activating mutation G158A *in vitro*. Quantities of 50 pg of various STING constructs were transfected into 30,000 cells. cGAMP at various concentrations was used to activate STING. SAVI-causing mutations are labeled in red, and other R281 mutations are labeled in green. *An *asterisk* above the *white bar* designating 0 μg/mL of cGAMP indicates a significant change ($P < .0001$) compared with the wild-type (WT) nontreated cells (indicated by the *white bar*), as determined by the use of ordinary 1-way ANOVA (Dunnett multiple comparisons tests). An asterisk above the *black bar* designating 20 μg/mL of cGAMP indicates a significant change ($P < .003$) of cells treated with 20 μg/mL of cGAMP compared with the respective nontreated cells (indicated by the respective *white bar*), as determined by the use of 2-way ANOVA (Bonferroni multiple comparisons tests). Data are presented as means ± SDs of duplicates. Similar results were obtained in independent experiments. **C,** A reconciled model to explain autoactivation of polymer interface mutations. The 2 subunits of STING dimer are shown in yellow and green. Polymer interfaces are indicated by *red boxes*. Inhibitors are shown as *gray ellipses*. The model assumes a putative inhibitor that is bound to the polymer interface and is unable to bind in patients with disease-causing mutation in either the connector helix loop region or in the polymer interface. For the full model and a detailed description, see also Fig E3. *EV*, Empty vector; *WT*, wild-type. *Modified with permission from Shang et al.*[E1]

mutations into hydrophobic amino acids such as tryptophan (W), leucine (L), or methionine (M), or into negatively charged amino acids (including glutamic acid [E]), cause autoactivation (Fig 2, *A* and *B*). The autoactivation was not due to differential protein expression in the transfection assay (see Fig E2 in this article's Online Repository at www.jacionline.org). The R281 and R284 mutations that were assessed remained responsive to cGAMP stimulation (Fig 2, *B* and see Fig E1), indicating no effect on ligand binding. The broad autoactivation of the R281 and R284 mutations was consistent with the model of polymer interface binding to an inhibitor to suppress STING autoactivation.[9] Although this potential inhibitor is not addressed in the 180° rotation model of the connector helix loop mutations, it is quite likely that the 180° rotation also leads to loss of inhibitor binding on the polymer interface, thus allowing side-by-side packing. Our data thus suggest a possible common mechanism to reconcile the 2 previously reported structural models (Fig 2, *C* and see also the Discussion section for detailed description of the model shown in Fig E3 in this article's Online Repository at www.jacionline.org), which is supported by similar superactivating mutations in both the connector helix loop (G158A) and the polymer interface (R281E, R284G, and R284S).

In summary, we have reported 6 patients from 4 unrelated families with recessively inherited *STING1* variants and characteristic clinical features of SAVI. Our data support the notion that the disease-causing homozygous p.R281W variant causes GOF but is weaker in activating STING than the previously reported heterozygous variants, and it requires biallelic mutations to constitutively activate STING. We have demonstrated a critical role of residue R281 in maintaining STING in an inactive state, likely without affecting dimer conformation. Our data unveil limitations of the current structural models that cannot explain the superactivating potential of the R281 and R284 mutations and raise questions as to whether class 3 residues represent an autoinhibitory domain or a binding site for an external inhibitor of STING. Considering the critical function of R281 and the nearby region, novel therapeutic options may arise from high-throughput screens of drugs that bind to this area and inhibit polymerization.

We thank the patients and their families for participating in this study.

Bin Lin, PhD[a]*
Roberta Berard, MD, MSc[b]*
Abdulrahman Al Rasheed, MD, MBBS, CAPB[c]*
Buthaina Aladba, MD, MBBS, CAPB[d]*
Philip J. Kranzusch, PhD[e,f]
Maggie Henderlight, BS[g]
Alexi Grom, MD[g]
Dana Kahle, BS[a]
Sofia Torreggiani, MD[a]
Alexander G. Aue[a]
Jacob Mitchell, BS[a]
Adriana A. de Jesus, MD, PhD[a]
Grant S. Schulert, MD, PhD[g]‡
Raphaela Goldbach-Mansky, MD, MHS[a]‡

From [a]the Translational Autoinflammatory Diseases Section, Laboratory of Clinical Immunology and Microbiology, National Institute of Allergy and Infectious Diseases, Bethesda, Md; [b]the Department of Pediatrics, Western University, London, Ontario, Canada; [c]the Division of Rheumatology, Pediatric Department, King Abdullah Specialized Children Hospital, King Abdulaziz Medical City, Riyadh, Saudi Arabia; [d]the Sidra Medical and Research Center, Department of Pediatric Medicine, Division of Rheumatology, Doha, Qatar; [e]the Department of Microbiology, Harvard Medical School, Boston, Mass; [f]the Department of Cancer Immunology & Virology, Dana-Farber Cancer Institute, Boston, Mass; and [g]the Cincinnati Children's Hospital Medical Center and Department of Pediatrics, University of Cincinnati College of Medicine, Cincinnati, Ohio. E-mail: goldbacr@mail.nih.gov.

*These authors share co-first authorship.

‡These authors contributed equally to this work.

This research was supported by the Intramural Research Program of the National Institutes of Health (NIH), National Institute of Allergy and Infectious Diseases (to R.G.-M.); grant K08 AR072075 (to G.S.S.) from NIH, National Institute of Arthritis, Musculoskeletal and Skin Diseases; and an Academic Research and Clinical (ARC) grant from Cincinnati Children's Research Foundation (to A.G. and G.S.S.).

Disclosure of potential conflict of interest: R. Goldbach-Mansky has received grant support from SOBI, Regeneron, Novartis, and Eli Lilly. The rest of the authors declare that they have no relevant conflicts of interest.

REFERENCES

1. Ishikawa H, Ma Z, Barber GN. STING regulates intracellular DNA-mediated, type I interferon-dependent innate immunity. Nature 2009;461:788-92.
2. Ablasser A, Chen ZJ. cGAS in action: Expanding roles in immunity and inflammation. Science 2019;363.
3. Liu Y, Jesus AA, Marrero B, Yang D, Ramsey SE, Sanchez GAM, et al. Activated STING in a vascular and pulmonary syndrome. N Engl J Med 2014;371:507-18.
4. Jeremiah N, Neven B, Gentili M, Callebaut I, Maschalidi S, Stolzenberg MC, et al. Inherited STING-activating mutation underlies a familial inflammatory syndrome with lupus-like manifestations. J Clin Invest 2014;124:5516-20.
5. Melki I, Rose Y, Uggenti C, Van Eyck L, Fremond ML, Kitabayashi N, et al. Disease-associated mutations identify a novel region in human STING necessary for the control of type I interferon signaling. J Allergy Clin Immunol 2017;140:543-52.e5.
6. Kim H, de Jesus AA, Brooks SR, Liu Y, Huang Y, VanTries R, et al. Development of a validated interferon score using nanostring technology. J Interferon Cytokine Res 2018;38:171-85.
7. Shang G, Zhang C, Chen ZJ, Bai XC, Zhang X. Cryo-EM structures of STING reveal its mechanism of activation by cyclic GMP-AMP. Nature 2019;567:389-93.
8. Konno H, Chinn IK, Hong D, Orange JS, Lupski JR, Mendoza A, et al. Pro-inflammation associated with a gain-of-function mutation (R284S) in the innate immune sensor STING. Cell Rep 2018;23:1112-23.
9. Ergun SL, Fernandez D, Weiss TM, Li L. STING polymer structure reveals mechanisms for activation, hyperactivation, and inhibition. Cell 2019;178:290-301.e10.

Available online July 13, 2020.
https://doi.org/10.1016/j.jaci.2020.06.032

A rare case of selective Igκ chain deficiency: Biologic and clinical implications

To the Editor:

Selective Igκ and Igλ deficiencies are extremely rare. So far, there have been few reported cases of Igκ deficiency in the English literature, and all but 2 of them are partial in nature.[1-3] The first reported case of complete Igκ deficiency was that of a male patient with concurrent cystic fibrosis, diabetes mellitus, malabsorption, and IgA deficiency[4]; notably, 1 of the patient's sisters had only trace amounts of κ^+ immunoglobulins. Sequencing of the κ constant region (*IGKC*) in this patient identified a different single-point mutation in each allele, p.Trp41Arg and p.Cys87Gly, each of which would disrupt stable κ chain folding.[5] The second published case was that of a 62-year-old female from southern Italy who had a history of recurrent respiratory infections and intestinal disorders from early childhood and was homozygous for the p.Cys87Gly point mutation observed in the original patient.[6]

Our patient is a 73-year-old white female; she is a retired nurse who has peripheral neuropathy but is otherwise healthy and with no history of immunodeficiency; nor is there any recorded history

METHODS

Patients

All patients were enrolled into the institutional review board–approved National Institutes of Health natural history protocol Studies of the Natural History, Pathogenesis, and Outcome of Autoinflammatory Diseases (NOMID/CAPS, DIRA, CANDLE, SAVI, NLRC4-MAS, Still's-like Diseases, and Other Undifferentiated Autoinflammatory Diseases) (17-I-0016; NCT02974595). Parents gave written informed consent for their children in accordance with the Declaration of Helsinki.

IFNB1 luciferase reporter assay

HEK293T cells were cotransfected with STING constructs and an *IFNB1* firefly luciferase reporter construct with Lipofectamine 3000 reagent (ThermoFisher Scientific, Waltham, Mass; catalog no. L3000015) in 96-well plates (black wall with clear bottom [BD Falcon, Frankin Lakes, NJ; catalog no. 353219]) with a reverse transfection protocol. Briefly, for 1 well of 96-well plate, 0.5 μL of *IFNB1* firefly luciferase reporter construct (100 ng/μL) was mixed with 5 μL of Opti-MEM, 0.2 μL of P300 reagent, and various amounts of STING constructs (6.25-400 pg in a volume of 0.25-0.4 μL), as indicated. The vector dilutions were then mixed with the Lipofectamine 3000 dilutions containing 5 μL of Opti-MEM and 0.3 μL of Lipofectamine 3000 and subsequently incubated at room temperature for 10 to 30 minutes. During the incubation period, HEK293T cells were harvested by trypsin digestion and diluted in complete Dulbecco modified Eagle medium to a density of 400,000 cells/mL. The transfection mix was applied to the wells following the incubation, after which 75 μL of diluted HEK293T cells (30,000 cells) was added to each well. To mix, the plate was gently tapped and then rocked back and forth to allow even distribution of the cells, followed by 10 minutes of incubation at room temperature to allow the cells to settle. The plates were then returned to 37°C in a humidified atmosphere with 5% CO_2 for 24 hours. The luciferase assay was carried out by using the ONE-Glo EX Luciferase Assay System (Promega, Madison, Wis; catalog no. E8120), with 50 μL of luciferase reagent per well.

cGAMP stimulation

For cGAMP stimulation, 1.8 μL of cGAMP (1 μg/μL) was diluted with 3.2 μL of complete Dulbecco modified Eagle medium and added to 1 well (of a 96-well plate) containing 85 μL of cultured HEK 293 T cells at 6 hours after transfection for a final concentration of 20 μg/mL.

Western blot

Transfection was carried out as already described except that 24-well plates were used (Corning Costar, Corning, NY; catalog no. 3524) and reagents and cells were added in quantities 4 times larger than in the 96-well plate. Briefly, 800 pg of STING construct and 200 ng of *IFNB1* firefly luciferase reporter construct were cotransfected into 120,000 HEK293T cells in each well.

Cells were harvested at 24 hours after transfection and were first washed with 1 mL of PBS, after which 50 μL of complete radioimmunoprecipitation assay (RIPA) buffer (composed of 9 mL of distilled water and 1 mL of 10× RIPA buffer [Cell Signaling Technology, Danvers, Mass; catalog no. 9086]; 1 tablet of cOmplete, Mini, EDTA-free Protease Inhibitor Cocktail [Roche Applied Science, Penzberg, Germany; catalog no. 11836170001]; 1 tablet of PhosSTOP phosphatase inhibitor [Roche Applied Science, catalog no. 4906837001]; and 0.125 g of *N*-ethylmaleimide [Sigma, St Louis, Mo; catalog no. E3876]) was added. The mixture was placed on ice for 10 minutes to lyse the cells. The lysate was collected into a 1.5-mL tube, vortexed for 15 seconds, and then spun at 17,000 *g* at 4°C for 10 minutes. The supernatant was transferred to a new tube. Protein concentrations were measured by using a DC protein assay kit (BIO-RAD, Hercules, Calif; catalog no. 5000116) with BSA as a standard. All samples were diluted to the same concentration with complete RIPA buffer, then mixed with NuPAGE Sample Reducing Agent (10X) (Invitrogen, Carlsbad, Calif; catalog no. NP0004) and XT Sample Buffer (4X) (BIO-RAD, catalog no. 1610791), and then heated at 70°C for 10 minutes.

For each sample, 12 μg of protein was loaded in 10% Criterion XT Bis-Tris Protein Gel (BIO-RAD, catalog no. 3450112) and electrophoresis was carried out in 3-(*N*-morpholino)propanesulfonic acid buffer (BIO-RAD, catalog no.1610793) by using Criterion Cell (BIO-RAD, catalog no. 1656001) at 200 V constant voltage for about 60 minutes. Next, 150 μL of NuPAGE Antioxidant (Invitrogen, catalog no. NP0005) was applied to the upper chamber buffer before the electrophoresis.

The proteins were transferred to polyvinylidene difluoride membranes (Trans-Blot Turbo Midi PVDF Transfer Packs, BIO-RAD, catalog no. 1704157) with the Trans-Blot Turbo Transfer System (BIO-RAD, catalog no.1704150) under the preprogrammed protocol for One Midi Format gel with a mixed molecular weight (2.5 A and ≤25 V for 7 minutes). The blots were then incubated and washed with gentle agitation (50 rpm) with Labnet Orbit low speed lab shaker (Labnet International, Edison, NJ; catalog no. S2030-LS-B) as detailed here. First, the blots were incubated in 20 mL of blocking buffer (5% nonfat dry milk, 1× Tris-buffered saline [TBS], and 0.1% Tween-20) at room temperature for 1 hour. Then they were washed for 5 minutes 3 times with about 20 mL of washing buffer (1× TBS and 0.1% Tween-20); followed by incubation in 0.2 μg/mL of anti-STING antibody (R&D Systems, Minneapolis, Minn; catalog no. MAB7169-SP) diluted in 12 mL of primary antibody dilution buffer (5% BSA, 1× TBS, and 0.1% Tween-20) at 4°C overnight with gentle agitation. The blot was then washed with washing buffer for 10 minutes 3 times, followed by 1 hour of incubation at room temperature in 12 mL of blocking buffer containing 6 μL of secondary antibody (Amersham ECL Sheep anti-Mouse IgG, Horseradish Peroxidase–Linked Whole Antibody, catalog no. NA931-1ML) and 12 μL of hFAB rhodamine anti-actin primary antibody (BIO-RAD, catalog no. 12004163). To remove any unbound antibodies, the membranes were washed for 10 minutes 3 times, after which SuperSignal West Dura Extended Duration Substrate (ThermoFisher Scientific, catalog no. 34076) was applied. Images for STING1 and ACTB were captured with BIO-RAD ChemiDoc.

DISCUSSION

STING detects microbial dinucleotides and functions as an adaptor molecule in the cytosolic DNA-sensing pathway that binds cGAMP, which is generated when cytosolic DNA activates cyclic cGAS.[E2-E6] The observed GOF of the STING autoactivating and disease-causing mutations was recently "explained" on the basis of 2 structural models.[E1,E7] The cryoelectron microscopy structure model suggests that cGAMP binding to the STING dimer causes a 180° rotation of the ligand-binding domain along a connector helix loop. This flattens the polymerization interfaces and enables side-by-side packing of STING dimers into polymers[E1] that serve as a platform for TBK1 cross-phosphorylation and subsequent signaling activation.[E8] Mutations of residues in the connector helix loop are referred to as class 1 SAVI mutations and include p.N154S and p.V155M (see Fig 1, *G* in the print text). These mutations favor a remodeling of the STING dimer structure into an autoactivated conformation. This model, however, cannot explain the mechanism of autoactivation of class 3 mutations in the polymer interface, including p.R281Q, p.R284G, and p.R284S, which are not predicted to induce remodeling of the STING dimer.

Another structural model proposes that residues in the polymer interface bind a C-terminal tail, which blocks STING polymerization.[E7] The class 3 SAVI mutations might therefore lose the ability to bind the C-terminal tail or an inhibitor (the latter is shown in the model) and cause autoactivation. Despite the differences between the 2 models, both converge at a conformational change in the polymer interface and STING activation.

Our data in fact suggest a possible common mechanism to reconcile the 2 previously reported structural models. The broad autoactivation of R281 and R284 mutations strongly suggests that the polymer interface binds to an inhibitor to suppress STING

autoactivation. On the basis of this reasoning, cGAMP binding to STING may not simply "flatten" the polymer interface but may also lead to loss of inhibitor binding capability as a result of the structural change in the polymerization interface (in the top panel Fig E3,[E1-E7] the inhibitors [which bind to the 2 dimer subunits on the front and back, respectively] are shown in black). This allows 180° rotation and STING polymerization. Similarly, STING dimers with class 1 mutations mimic the cGAMP-bound STING structure and lost inhibitor binding, which leads to activation (in the middle panel of Fig E3, the location of connector helix loop is indicated by a red box).

Our hypothetical model likely explains the higher autoactivation threshold for class 3 mutations than for class 1 mutations. On the basis of the current structural model, V155 is located in the closely packed dimer interface, and mutations into a methionine (M) change the molecular interactions inside the dimer, favoring an active dimer conformation.[E1] This conformational change can even happen in the wild-type/mutant heterodimers, which is supported by the fact that V155M mutations are disease causing in heterozygosity and show a lower autoactivation threshold than class 3 mutations, including R281Q, R284S, and R284G (see also Fig 2, A and B). In contrast, for class 3 mutations in the polymer interface (indicated by a red box in the bottom panel of Fig E3), only the mutant-mutant homodimers are able to fully resolve the inhibitor blocking on both sides of the STING dimer (Fig E3, bottom panel). Consistent with this hypothesis, the class 3 mutations either require homozygosity to be disease causing (eg, p.R281W) or they need to be superautoactivating to cause SAVI in heterozygosity (eg, R281Q, R284S, and R284G). Further structural studies of the class 3 superautoactivating mutations are required to test this hypothesis and enhance our understanding of STING activation. Considering the reports of the STING C-terminal tail functioning as an autoinhibitory suppressor[E7] and discoveries of other STING binding partners, including TOLLIP, IRE1α,[E9] and STIM1,[E10] it remains to be determined whether these STING-binding proteins/domains represent various STING inhibitors or form a single suppressor complex.

REFERENCES

E1. Shang G, Zhang C, Chen ZJ, Bai XC, Zhang X. Cryo-EM structures of STING reveal its mechanism of activation by cyclic GMP-AMP. Nature 2019;567:389-93.

E2. Sun L, Wu J, Du F, Chen X, Chen ZJ. Cyclic GMP-AMP synthase is a cytosolic DNA sensor that activates the type I interferon pathway. Science 2013;339:786-91.

E3. Gao P, Ascano M, Wu Y, Barchet W, Gaffney BL, Zillinger T, et al. Cyclic [G(2',5')pA(3',5')p] is the metazoan second messenger produced by DNA-activated cyclic GMP-AMP synthase. Cell 2013;153:1094-107.

E4. Diner EJ, Burdette DL, Wilson SC, Monroe KM, Kellenberger CA, Hyodo M, et al. The innate immune DNA sensor cGAS produces a noncanonical cyclic dinucleotide that activates human STING. Cell Rep 2013;3:1355-61.

E5. Ablasser A, Goldeck M, Cavlar T, Deimling T, Witte G, Rohl I, et al. cGAS produces a 2'-5'-linked cyclic dinucleotide second messenger that activates STING. Nature 2013;498:380-4.

E6. Zhang X, Shi H, Wu J, Zhang X, Sun L, Chen C, et al. Cyclic GMP-AMP containing mixed phosphodiester linkages is an endogenous high-affinity ligand for STING. Mol Cell 2013;51:226-35.

E7. Ergun SL, Fernandez D, Weiss TM, Li L. STING polymer structure reveals mechanisms for activation, hyperactivation, and inhibition. Cell 2019;178:290-301.e10.

E8. Zhang C, Shang G, Gui X, Zhang X, Bai XC, Chen ZJ. Structural basis of STING binding with and phosphorylation by TBK1. Nature 2019;567:394-8.

E9. Pokatayev V, Yang K, Tu X, Dobbs N, Wu J, Kalb RG, et al. Homeostatic regulation of STING protein at the resting state by stabilizer TOLLIP. Nat Immunol 2020;21:158-67.

E10. Srikanth S, Woo JS, Wu B, El-Sherbiny YM, Leung J, Chupradit K, et al. The Ca(2+) sensor STIM1 regulates the type I interferon response by retaining the signaling adaptor STING at the endoplasmic reticulum. Nat Immunol 2019;20:152-62.

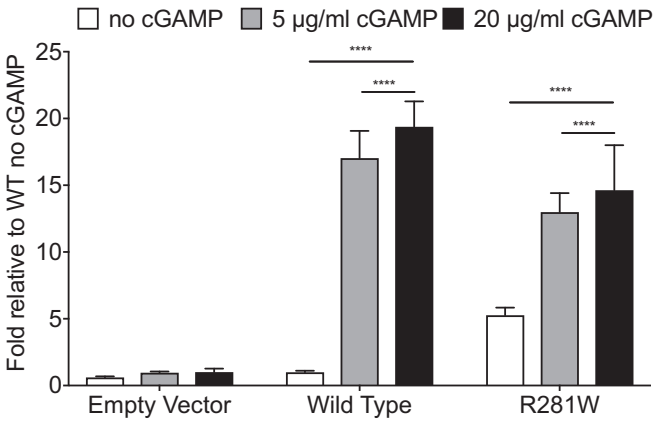

FIG E1. The R281W mutant is autoactivating and remains responsive to cGAMP stimulation. Quantities of 50 pg of various STING constructs were transfected into 30,000 HEK293T cells and stimulated with cGAMP at 6 hours after transfection. ****$P < .0001$ by 2-way ANOVA and the Dunnett multiple comparison test. *WT*, Wild-type.

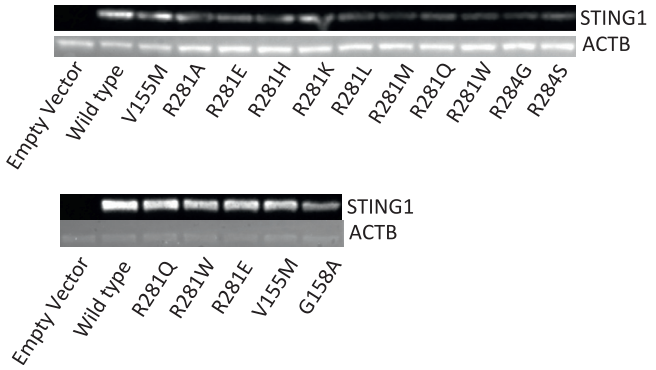

FIG E2. Protein expression of transfected constructs in HEK293T cells by Western blot. *STING1*-expressing constructs (800 pg) were transfected into 120,000 HEK293T cells, and STING1 and ACTB were detected in chemiluminescent and rhodamine channels, respectively, in the same blot.

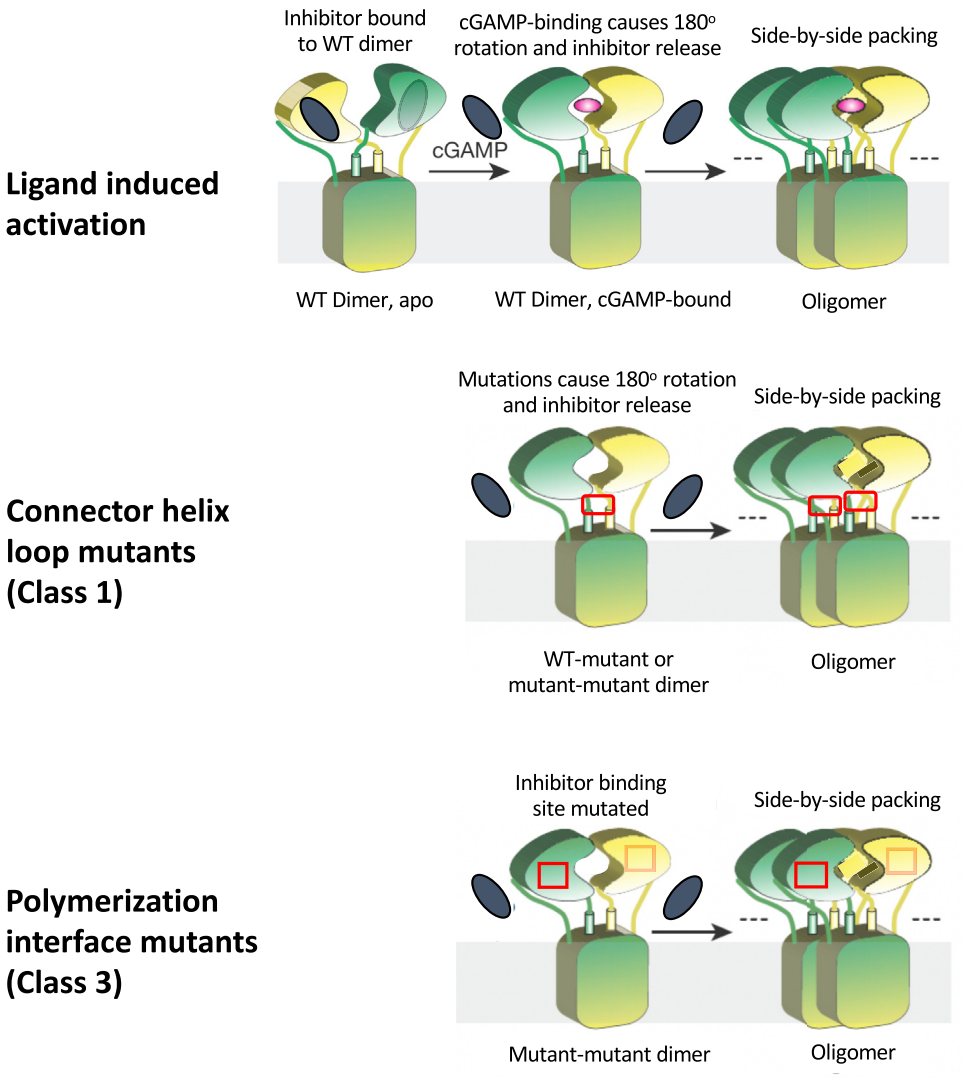

FIG E3. Proposed disease models for class 1 and class 3 mutations. The 2 subunits of the STING dimer are shown in yellow and green. Sites of SAVI-causing mutation are indicated by *red boxes*. Inhibitors are shown as a *gray ellipse*. The model assumes that a putative inhibitor is bound to the polymer interface of the wild-type STING dimer, which blocks the polymer formation. cGAMP-binding to the binding domain of STING *(top panel)* or mutations in the connector region *(middle panel)* cause a 180° rotation of the ligand-binding domain along the connector helix loop, which leads to the release of the inhibitor. This allows polymer formation via side-by-side packing and STING activation. Mutations in the polymer interface *(bottom panel)* directly lead to inability of inhibitor binding, which causes STING autoactivation. *WT*, Wild-type. Modified with permission from Shang et al.[E1]

TABLE E1. Clinical and laboratory findings and outcomes of patients with homozygous *STING1* c.841C>T, p.R281W

Patient no.	Age at presentation	Nationality	Cutaneous features	Pulmo-nary involvement	Chest CT findings	Other clinical features	Autoantibodies	Other laboratory findings	Current treatment/ status
1	4 wk	Syrian	Yes	Yes	Diffuse bilateral parenchymal opacities	Failure to thrive	ANA positive	Elevated CRP level, ESR, anemia	Died at age 5 mo
2	Unknown	Syrian	Unknown	Yes	ND	Unknown	Unknown	Unknown	Died at age 18 mo
3	3 mo	Saudi	Yes	Yes	Interstitial lung disease, enlarged mediastinal lymph nodes	GERD, vomiting, diarrhea, failure to thrive, clubbing	ANA positive, ANCA positive (anti-PR3)	Elevated CRP level; ESR; and IgG, IgA, and IgM levels	Treated with ruxolitinib with a favorable response
4	6 mo	Saudi	Yes (facial rash)	Yes	Interstitial lung disease and enlarged mediastinal lymph nodes	Delayed gross motor development, failure to thrive, short stature, clubbing	ANA positive, anti-dsDNA–positive, ANCA positive (MPO)	Elevated CRP level, ESR, and IgG level	Treated with baricitinib with a favorable response
5	2 mo	Qatar	Yes	Yes	Reticulonodular densities throughout, pulmonary hypertension, and enlarged hilar and mediastinal lymph nodes	Polyarthritis, clubbing, pulmonary hypertension	ANA positive, c-ANCA–positive	Elevated CRP level, ESR, and IgG level; anemia; leukopenia	Treated with baricitinib with a favorable response
6	8 mo	Syrian	Yes	Yes	Cystic lesions, RUL fibrosis	Polyarthritis, clubbing, failure to thrive, hair loss	ANA positive, c-ANCA positive	Elevated CRP level, ESR, elevated IgG and IgM levels; anemia; additional genetic finding*	Treated with baricitinib with a favorable response

ANA, Antinuclear antibody; *ANCA*, antineutrophil cytoplasmic antibody; *anti-PR3*, anti-proteinase 3 antibody; *c-ANCA*, cytoplasmic antineutrophil cytoplasmic antibody; *CRP*, C-reactive protein; *CT*, computed tomography; *dsDNA*, double-stranded DNA; *ESR*, erythrocyte sedimentation rate; *GERD*, gastroesophageal reflux disease; *MPO*, myeloperoxidase; *ND*, not done; *RUL*, right upper lobe.
*Patient 5 had a heterozygous mutation in *ADA2*/*CECR1*, but with normal enzymatic levels.